Probe Design Optimization for Time-Domain NIROT "Pioneer" System for Imaging the Oxygenation of the Preterm Brain

Di Costanzo-Mata, A.; Jiang, J.; Lindner, S.; Zhang, C.; Charbon, E.; Wolf, M.; Kalyanov, A.

DOI
10.1007/978-3-030-48238-1_57

Publication date
2021

Document Version
Final published version

Published in
Oxygen transport to Tissue XLII

57

Probe Design Optimization for Time-Domain NIROT "Pioneer" System for Imaging the Oxygenation of the Preterm Brain

A. Di Costanzo-Mata, J. Jiang, S. Lindner, C. Zhang, E. Charbon, M. Wolf, and A. Kalyanov

Abstract

In preterm infants, there is a risk of life-lasting impairments due to hemorrhagic/ischemic lesions. Our time-domain (TD) near-infrared optical tomography (NIROT) system "Pioneer" aims at detecting both disorders with high spatial resolution. Successfully tested on phantoms, "Pioneer" entered the phase of improvements and enhancements. The current probe (A-probe) was adapted for an optoacoustics instrument. A new probe (B-probe) optimized for TD measurements is required. Our aim is to determine the optimal arrangement of light sources in the B-probe to increase the sensitivity and the resolution of Pioneer and to improve the ability of the system to detect both ischemia and hemorrhage. To do this, we simulated TD-NIROT signals in NIRFAST, a MATLAB-based package used to model near-infrared light propagation through tissue. We used 16 × 16 detector array, with ~2.2 mm distance between the detectors. Light sources were arranged around the field of view (FoV). We performed forward simulations of light propagation through a "homogeneous case" (HC) tissue ($\mu'_s = 5.6\ cm^{-1}$, $\mu_a = 0.07\ cm^{-1}$). Next, we simulated light propagation through "inhomogeneous case" -tissue' (IC) tissue by adding ischemia ($\mu_a = \mu_a \cdot 2.5\ cm^{-1}$) or hemorrhage ($\mu_a = \mu_a \cdot 50\ cm^{-1}$) to HT as a spherical inclusion of 5 mm radius at different depths in the FoV center and identified the source location that provides the higher contrast on the FoV: $\max_{i \in I}$ ($FoVContrast_{SOURCE}$). It was found that sources located closer to the FoV center generate greater contrast for late photons. This study suggests the light sources in B-probe should be closer to the FoV center. The higher sensitivity is expected to lead to a higher image quality.

A. Di Costanzo-Mata (✉) · J. Jiang · M. Wolf
A. Kalyanov
Biomedical Optics Research Laboratory (BORL), Department of Neonatology, University of Zurich and University Hospital Zurich, Zurich, Switzerland
e-mail: aldo.dicostanzomata@usz.ch

S. Lindner
Biomedical Optics Research Laboratory (BORL), Department of Neonatology, University of Zurich and University Hospital Zurich, Zurich, Switzerland

Advanced Quantum Architecture (AQUA), Laboratory, School of Engineering, EPFL Lausanne, Lausanne, Switzerland

C. Zhang
Applied Quantum Architectures, Delft University of Technology, Delft, the Netherlands

E. Charbon
Advanced Quantum Architecture (AQUA) Laboratory, School of Engineering, EPFL Lausanne, Lausanne, Switzerland

E. M. Nemoto et al. (eds.), *Oxygen Transport to Tissue XLII*, Advances in Experimental Medicine and Biology 1269, https://doi.org/10.1007/978-3-030-48238-1_57

Keywords

Near-infrared optical tomography (NIROT) · Time-domain imaging · Tissue oxygenation · Time-domain simulations · Time-domain NIROT

57.1 Introduction

Worldwide, ~15 million infants are born preterm every year, and this number is rising. This represents ~10% of the total births [1]. Preterm infants are delicate, and in particular, the brain is vulnerable to lesions, and these do not heal well. Long-term cognitive, sensory, motor, and/or behavioral impairments affect up to ~50% of preterm born patients at school-age [2]. In addition, these lifetime disabilities may lead to significant healthcare costs [3]. Brain lesions are probably often caused by hypoxia or hyperoxia, which may lead to hemorrhage and infarction and ultimately white matter injuries (WMI).

Magnetic resonance imaging (MRI) is a powerful neuroimaging tool for detecting brain structural lesions, i.e., white matter injury [4]. Nonetheless, MRI is unable to detect hypoxia or ischemia causing the WMI. In addition, MRI requires a risky transport of these delicate patients. Therefore, a bedside method is required. Ultrasound (US) is a bedside instrument and detects hemorrhagic lesions immediately. However, US is unable to measure oxygenation and detect hypoxia.

Near-infrared spectroscopy (NIRS) detects hyperoxia, hypoxia, or ischemia, but it is not spatially specific. Near-infrared optical tomography (NIROT) is still at the research stage, but has the potential to fulfill all the requirements, i.e., to become a bedside tool able to measure the oxygenation with high-spatial resolution [5]. Therefore, it is expected to the early detect and possibly prevent hemorrhage, hypoxia, and ischemia.

Recently, we introduced "Pioneer" as a time-domain (TD) NIROT imaging system [6]. Tests detecting ischemic-like inclusions inside phantoms have been successful. Now, "Pioneer" has entered the phase of improvements and enhancements.

The current Pioneer probe (A-probe setup) comprises a ring structure with 11 sources ~23 mm away from the field-of-view (FoV) center. The FoV has 32 × 32 SPAD detectors array (camera), with ~1.1 mm distance between the detectors. The A-probe was adapted from a multimodal optoacoustic-NIROT instrument [7].

A new optimized Pioneer probe (B-probe) is required to increase the sensitivity to the late-arriving photons (LAPs) [8], which will enable higher image quality and sensitivity to deep hemorrhage, hypoxia, or ischemia.

The aim is to investigate the optimal arrangement of light sources in the B-probe to increase the sensitivity for LAPs, hemorrhage, and hypoxia.

57.2 Method

The metric which we used to identify which source locations will enhance the signal sensitivity was the contrast ratio between the time-point spread functions (TPSF) and, in particular, the LAPs, from a simulated "healthy" tissue, i.e., a homogeneous case (HC), against tissue including a localized ischemia or hemorrhage, an inhomogeneous case (IC).

The light propagation in tissue was simulated by NIRFAST [9]. A mesh was generated to mimic tissue and to implement the FoV of Pioneer (detectors set). The mesh has dimensions of 100 × 100 × 50 mm ("xyz-axis") with 0.6 mm nodal distance. Virtual detectors (D) were placed as a 16 × 16 squared grid at "$z = 0$" and centered over the "xy-axis." Detectors were separated by 2.2 mm between them $\{D \in N^{256} | D = (1, \cdots, 256)\}$. Nine virtual sources (S) were placed covering an octant external to the FoV $\{S \in N^{9} | S = (1, \cdots, 9)\}$ (Fig. 57.1a). The mesh optical properties were $\mu'_s = 5.6\ cm^{-1}$ and $\mu_a = 0.07\ cm^{-1}$, which are optical properties of an infant's head for the HC [10]. Ischemia ($\mu_{a\ ischemia} = \mu_{a\ HC} \cdot 2.5$) and hemorrhage ($\mu_{a\ hemorrhage} = \mu_{a\ HC} \cdot 50$) were modeled as spherical inclusions of 10 mm diam-

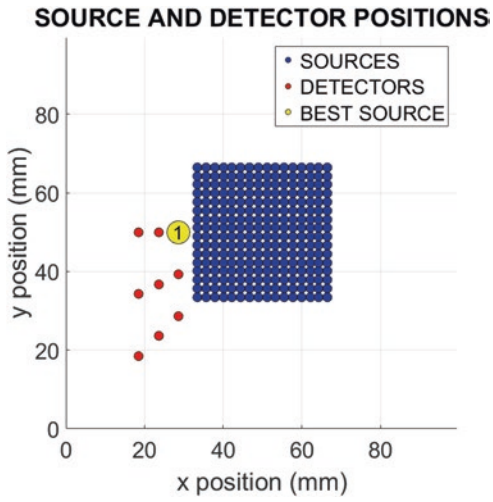

Fig. 57.1 Simulated mesh sources and detector positions. In blue, 16 × 16 squared grid of detector array with 2.2 mm separation distance between them. In red, nine sources with 5 mm x-axis equidistant separation between them. Highlighted in yellow, the selected source locations yielding a greater contrast for different ischemic inclusion depth (Table 57.1) and for hemorrhagic inclusions (Table 57.2)

eter. Mesh simulations with these inclusions represent the IC. Each IC mesh has an inclusion placed at a different depth below the center of the FoV.

NIRFAST TD computational modeling generated TPSF data for the HC and IC. The simulations covered a 6 ns time window with a sampling rate of 0.1 ns, resulting in 61 time-bins (TB), $\{TB \in R^{61} | TB = (0, 0.1, \cdots, 6)\}$. We considered the LAPs to be present in the time-bins from TB_{29} = 2.8 ns to TB_{61} = 6 ns, $\left\{LAPs \in I^{33} \mid LAPs = (29, \cdots, 61)\right\}$. The LAP's interval represents the photons reaching ~15 mm depth and below [11].

To calculate the intensity I over the time interval of the LAPs, we employ

$$I_{TPSF_{S,D,TB}}(LAPs) = \sum_{LAPs} TPSF_{S,D,TB_{LAPs}}, \quad (57.1)$$

where S is the selected source, D is the selected detector, and TPSF represents the simulated TD data matrix $\{TPSF_{S,D,TB} \in R^{9,256,61}\}$.

The contrast C represents a percentage difference between the IC intensity (I_{IC}) and the HC intensity (I_{HC}) in the time interval of the LAPs:

$$C_{S,D}(LAPs) = 1 - \frac{I_{IC_{S,D,TB}}(LAPs)}{I_{HC_{S,D,TB}}(LAPs)}. \quad (57.2)$$

The FoV contrast (FoVC) is the summated contrasts from all the detectors regarding a single source S in the time interval of the LAPs:

$$FoVC_S(LAPS) = \sum_D C_{S,D}(LAPs) \quad (57.3)$$

The FoVC yielding the greatest value, among the $FoVC_S(LAPS)$ vector's values, determines the "selected source S" that generates the greater contrast for our Pioneer system ($selected\ S = \max_{S \in I}(FoVC_S(LAPS))$). Such a "selected S" xyz-location is retrieved from the mesh design parameters (Fig. 57.1). Finally, we calculate the Euclidian distance of the "selected S" against the closest boundary to the FoV perimeter and to the FoV center. Such distances identify the location where the sources generate a higher system sensitivity to a deep inclusion below the FoV center.

57.3 Results

The simulations have sources placed from 21.43 mm to 44.44 mm away from the FoV center and 5.05 mm to 21.11 mm away from the FoV perimeter (edge). According to the index value obtained from $\max_{S \in I}(FoVC_S(LAPS))$, the most sensitive contrast for LAPs is for the sources near the FoV perimeter and to the FoV center. The "selected source" metrics for different ischemic inclusion depth are in Table. 57.1 and for hemorrhagic inclusions in Table 57.2 (Fig. 57.1).

To generate data diversity, three lines of three sources were simulated. The sources had 5 mm separation between them and away from the FoV in the x-axis. Each line of sources had an angular displacement of ∠22.5° starting at ∠180° relative to the FoV center. It was observed that sources located near the FoV perimeter deliver a higher $FoVC_S(LAPS)$ values (Fig. 57.2a), and the highest $FoVC_S(LAPS)$ was for the source nearest to the FoV center (Fig. 57.2b).

Table 57.1 Selected source S data table for ischemic inclusion at different depths (Fig. 57.1)

Inclusion depth	Selected S#	Max ($C_{S\#,D}$(LAPs))	S-FoV center dist.	S-FoV edge dist.	$FoVC_S$(LAPS)
10 mm	1	80.3%	21.43 mm	5.05 mm	~76.95
20 mm	1	72.2%	21.43 mm	5.05 mm	~66.19
25 mm	1	61.1%	21.43 mm	5.05 mm	~48.43
30 mm	1	39.0%	21.43 mm	5.05 mm	~30.64

Table 57.2 Selected source S data table for hemorrhagic inclusion at different depths (Fig. 57.1)

Inclusion depth	Selected S#	Max ($C_{S\#,D}$(LAPs))	S-FoV center dist.	S-FoV edge dist.	$FoVC_S$(LAPS)
10 mm	1	84.59%	21.43 mm	5.05 mm	~96.96
20 mm	1	87.43%	21.43 mm	5.05 mm	~85.79
30 mm	1	55.47%	21.43 mm	5.05 mm	~42.77
40 mm	1	14.41%	21.43 mm	5.05 mm	~11.06

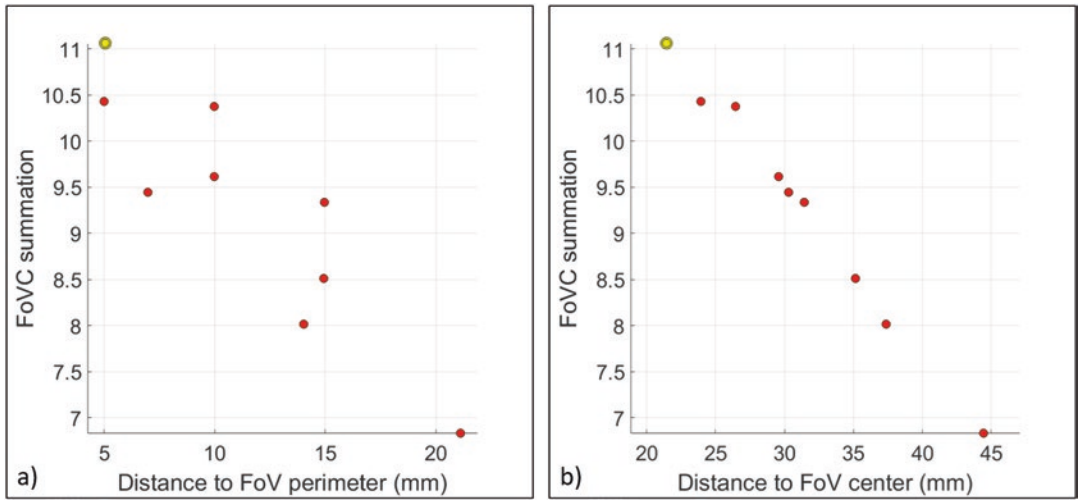

Fig. 57.2 Plot of summated contrast ratio (FoVC) for a hemorrhagic inclusion 40 mm deep (**a**) versus the distance of each source from the perimeter of the FoV (**b**) versus the distance of each source from the center of the FoV. Each source is represented as a red dot. In yellow is the selected source yielding a greater contrast

57.4 Discussion

Pioneer time-domain data enables to resolve deeper anomalies (~3 cm) in tissues, with short S-D distances (~2 cm), which is not possible by continuous-wave (CW) NIROT. This depth resolution is relevant, because tissue consists of layers with different optical properties (skin, skull, muscle, brain) and because it enables to obtain the optical properties of the layer of interest (e.g., the brain). This layered structure was not represented in our phantoms. However, due to the high contrast of the lesions (e.g., hemorrhage is 50 times more absorbant than the surrounding tissue), the difference between the other tissue layers may be neglected as a first approximation. The A-probe had a comparably long distance to the FoV of the detectors. For the B-probe, the sources were close (~5 mm) to the FoV perimeter. This small distance yielded the greatest contrast for all 1024 detectors. In addition, in the A

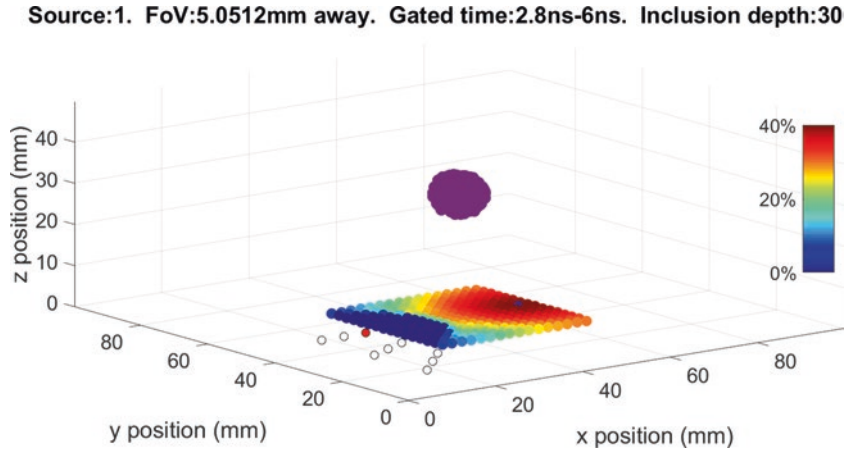

Fig. 57.3 Simulated contrast map in the field of view for an ischemic inclusion 30 mm deep for the source ~5 mm away from the detector edge and ~21.5 mm from the FoV center yielding the highest contrast ratio

probe a high number of 700 detectors was not sensitive to the light, i.e., inactive. The higher contrast and number of active detectors provides a higher signal-to-noise ratio and more information for the image reconstruction. The A-probe showed a contrast of ~20% for ischemia 30 mm deep using ~330 detectors [6]; with the B-probe, we achieved a contrast ~39% using 1024 detectors.

57.5 Conclusion

To achieve a high contrast for the LAPs, the B-probe sources must be close to the FoV perimeter and the center for ischemic or hemorrhage deep inclusions (Fig. 57.3). The higher sensitivity is expected to lead to a higher image quality.

Acknowledgments This research was supported by Swiss Cancer Research grant KFS-3732-08-2015, the Swiss National Science Foundation project 159490 and CONACyT by the CVU-627802. MW declares that he is president of the board and co-founder of OxyPrem AG.

References

1. Anderson P et al (2003) Neurobehavioral outcomes of school-age children born extremely low birth weight or very preterm in the 1990s. JAMA 289(24):3264–3272
2. World Health Organization (2018) Preterm birth. https://www.who.int/news-room/fact-sheets/detail/preterm-birth. Accessed 24 Jun 2019
3. Fanaroff AA et al (2007) Trends in neonatal morbidity and mortality for very low birthweight infants. Am J Obstet Gynecol 196(2):147–1e1
4. Lee YA (2017) White matter injury of prematurity: its mechanisms and clinical features. J Pathol Transl Med 51(5):449
5. Boas DA et al (2001) Imaging the body with diffuse optical tomography. IEEE Signal Process Mag 18(6):57–75
6. Di Costanzo-Mata A et al (2018) Time-resolved NIROT 'Pioneer' system for imaging oxygenation of the preterm brain: preliminary results. In: Ryu P, Lee S, Harrison D, LaManna J (eds) The 46th annual meeting of the International Society on Oxygen Transport to Tissue Proceedings. Springer, Cham, p 2018
7. Ahnen L et al (2017) Development and validation of a sensor prototype for near-infrared imaging of the newborn brain. In: Halpern H, LaManna J, Harrison D, Epel B (eds) Oxygen transport to tissue XXXIX. Advances in experimental medicine and biology, vol 977. Springer, Cham
8. Proskurin SG (2011) Using late arriving photons for diffuse optical tomography of biological objects. Quantum Electron 41(5):402
9. Jermyn M et al (2013) Fast segmentation and high-quality three-dimensional volume mesh creation from medical images for diffuse optical tomography. J Biomed Opt 18(8):086007
10. Arri SJ et al (2011) Precision of cerebral oxygenation and hemoglobin concentration measurements in neonates measured by near-infrared spectroscopy. J Biomed Opt 16(4):047005
11. Torricelli A et al (2005) Time-resolved reflectance at null source-detector separation: improving contrast and resolution in diffuse optical imaging. Phys Rev Lett 95(7):078101